Cellular Microbiology

WILEY

RESEARCH ARTICLE OPEN ACCESS

In Silico Investigation of Dual-Target Quorum Sensing Inhibitors to Eradicate Biofilm Formation in *Candida albicans*

Doha EL Meskini[1] | Fettouma Chraa[1] | Taoufiq Benali[2] | Rachid El Jaoudi[1] | Mouna Ouadghiri[1] | Abdelhakim Bouyahya[3] | Hooi Leng Ser[4] | Bey Hing Goh[5,6,7] | Tarik Aanniz[1]

[1]Medical Biotechnology Laboratory (MedBiotech), Bioinova Research Center, Medical and Pharmacy School, Mohammed V University in Rabat, Rabat, Morocco | [2]Laboratory of Ecotoxicology, Bioresources, and Coastal Geomorphology, Polydisciplinary Faculty of Safi, Cadi Ayyad University, Safi, Morocco | [3]Laboratory of Human Pathologies Biology, Faculty of Sciences, Mohammed V University in Rabat, Rabat, Morocco | [4]Faculty of Medical and Life Sciences, Sunway University, Petaling Jaya, Malaysia | [5]Faculty of Medical & Life Sciences, Sunway Biofunctional Molecules Discovery Centre, Sunway University, Petaling Jaya, Selangor, Malaysia | [6]Faculty of Health, Australian Research Centre in Complementary and Integrative Medicine, University of Technology Sydney, Ultimo, Australia | [7]Graduate Institute of Cancer Biology and Drug Discovery, College of Medical Science and Technology, Taipei Medical University, Taipei, Taiwan

Correspondence: Bey Hing Goh (goh.beyhing@uts.edu.au) | Tarik Aanniz (t.aanniz@um5r.ac.ma)

Received: 18 July 2025 | **Revised:** 29 March 2026 | **Accepted:** 9 May 2026

Academic Editor: Anirudha Chattopadhyay

Keywords: ADMET | biofilm | *C. albicans* | CYC | MD simulations | quorum sensing | RAS1

ABSTRACT

Candida albicans (*C. albicans*) is an opportunistic yeast that forms biofilms, which confer increased resistance to antifungal agents, making infections very difficult to treat. One of the mechanisms regulating this virulence is quorum sensing (QS), which can be defined as a cellular communication mechanism based on the production of autoinducer, namely, farnesol. We previously reported that the essential oils of *Cistus ladanifer*, *Matricaria chamomilla*, and *Pistacia lentiscus* inhibit *C. albicans*. In this context, a virtual screening of 48 molecules derived from these plants, as well as their ADMET property predictions, was undertaken to identify the most promising ligands for inhibiting QS receptors (CYC and RAS1) compared to farnesol. The latter exhibited a binding affinity of −7.0 kcal/mol for both CYC and RAS1. Two phytomolecules, namely, chamazulene and γ-muurolene, exhibited stronger binding affinities of −7.6 and −8.1 kcal/mol, respectively, for CYC, while toward the RAS1 receptor, they showed identical binding affinities of −7.1 kcal/mol. According to the binding free energy calculations performed using Prime MM-GBSA, the complexes formed by γ-muurolene exhibited high stability, maintained by coulombic, lipophilic, and Van der Waals interactions, demonstrating that γ-muurolene is a promising inhibitor of QS. Molecular dynamic simulations confirmed the conformational stability of the CYC-γ-muurolene and RAS1-γ-muurolene complexes, characterized by low RMSD values, suggesting favorable dynamic behavior. The results as a whole provide a solid foundation for further experimental validation.

1 | Introduction

Fungal infections cause a number of deaths similar to those caused by HIV or tuberculosis and a very high global mortality rate compared to deaths from breast cancer or malaria [1]. One of the main causative agents of fungal disorders in humans is *Candida albicans* (*C. albicans*). The latter is defined as a commensal fungus that naturally colonizes the surfaces of mucous membranes and skin. However, due to variations in environmental conditions, *C. albicans* becomes opportunistic (pathogenic) and can cause millions of skin and mucosal infections each year in the vagina, intestines, and mouth, and even serious

This is an open access article under the terms of the Creative Commons Attribution License, which permits use, distribution and reproduction in any medium, provided the original work is properly cited.

Copyright © 2026 Doha EL Meskini et al. *Cellular Microbiology* published by John Wiley & Sons Ltd.

systemic infections that can be potentially fatal [1, 2]. Besides, *C. albicans* is the fungal species most frequently isolated in clinical infections [3]. It has been found that the transition from the commensal state to the opportunistic state is due to the polymorphism (dimorphism) of this fungus. Otherwise, the ability of *C. albicans* to transform from the yeast form in blastospores to the filamentous, invasive form in hyphae, or pseudohyphae, is an important factor of virulence. This hyphal virulence is ascribed to its resistance to phagocytosis by immune cells. The hyphae adhere to surfaces and can easily invade the host and damage its tissues; they also contribute to the formation of biofilm [2–4]. Fungal biofilms rank fourth in terms of the frequency of bloodstream infections, while they have received significantly less attention [3]. *C. albicans* biofilms can be defined as complex three-dimensional structures formed by cells encased in an extracellular polymeric matrix, providing resistance to antifungal treatments; in other words, the biofilm's sensitivity to antifungals is low, as well as its resistance to immune responses [5, 6]. It has been demonstrated that *C. albicans* controls its morphological change, essential for biofilm formation, according to cell density, which is regulated through quorum sensing (QS) [2]. The latter refers to a process by which microorganisms adjust their behavior according to their population density using molecules called "autoinducers" (AIs), namely, farnesol, in *C. albicans*. At high cell density, farnesol inhibits yeast–hyphae transformation by blocking the RAS1-cAMP-PKA signaling pathway [7]. By binding to RAS1 (signaling GTPase) and CYC receptors, a catalytic domain of adenylate cyclase (CYR1), farnesol inhibits intracellular cAMP production, which subsequently prevents the activation of protein kinase (PKA) responsible for the activation of the CPH1 and HST7 genes essential for hyphae formation and the activation of hyphae suppressor gene expression, namely, HOG1 and TUP1 [8–12]. The inhibition of both QS regulators, a process called quorum quenching (QQ), is considered a promising therapeutic alternative to current ineffective antifungals [7, 13]. Spaggiari et al. deeply analyzed the patents and patent applications deposited between 2019 and 2023 related to QS inhibitors that could serve as antimicrobials in the future [14]. Collectively, ongoing researches and valuable outcomes support the therapeutic potential of QS as an alternative option for managing antimicrobial resistance without promoting it [15–23]. However, although there is much advancement in bacterial systems, this remains an underexplored area of research for antifungal pathogens such as *C. albicans*. Hence, QQ can be achieved by considering several strategies, including enzymatic QQ, which is based on the enzymatic degradation of bacterial signals while inactivating AIs before their detection by bacterial receptors, by using enzymes like lactonasea and acylases [24]. Other strategies focus on free AIs in the environment, by sequestering them either with synthetic antibodies such as AP4-24H11 [25, 26] or with cyclodextrins [25, 27]. Other promising approaches involve the use of molecules that mimic the structure of AIs and generate inactive analogs and natural QS-inhibiting molecules [25, 28, 29].

In our previous study, the essential oils (EOs) extracted from three medicinal plants, namely, *Cistus ladanifer*, *Matricaria chamomilla*, and *Pistacia lentiscus*, were found to inhibit the growth of *C. albicans* [30]. As the use of these pure molecules is the new paradigm of modern medicine and current drug discovery that tends to abandon the use of complex mixtures, we aimed to screen phytocompounds found in those EOs to select the best candidate that targets QS receptors in *C. albicans*, namely, CYC and RAS1 receptors, to address the problem of antifungal resistance in candidiasis.

2 | Materials and Methods

2.1 | Data Collection and Ligand Preparation

A database containing 48 molecules was constructed from three medicinal plants, namely, *C. ladanifer*, *M. chamomilla*, and *P. lentiscus*, which have already proven their antifungal activity against *C. albicans*. They were examined in order to select the most promising ligand molecules that inhibit the QS receptors CYC and RAS1 [7]. The 3D structures of the ligands were obtained from the PubChem database [31, 32] in SDF format, which will be converted to PDB format using Open Babel 3.1.1. The structures were then prepared using AutoDockTools (ADT Version 1.5.7) by adding Gasteiger charges and polar hydrogens and then saved in PDBQT format [33, 34].

2.2 | Receptor Retrieval, Homology Modeling, and Validation

The 3D structure of the RAS1 protein (ID: 7NZZ) was obtained from the Protein Data Bank (PDB ID: 7NZZ), while the 3D structure of the CYC protein is not available in the PDB database. However, a homology modeling process was used to generate it using SWISS-MODEL (https://swissmodel.expasy.org/interactive) [7]. The amino acid sequence of the CYC target was extracted from the UniProt Knowledgebase (UniProtKB) database in FASTA format (UniProt ID: Q9P977_CANAX) [7]. This sequence was inserted into SWISS-MODEL, which modeled the 3D structure of the protein based on the 3D structure of a homologous protein. Among the proposed 3D structures, we chose the one predicted by AlphaFold due to its high accuracy, as it predicts structures close to experimental methods [35]. It has a high predicted local distance difference test (pLDDT) score of 75.12, confirming good modeling and structural reliability [36, 37]. The predicted structure is distinguished by a Global Model Quality Estimate (GMQE = 0.76) close to 1 and a sequence identity of 99.70%, exceeding 50%, which confirms the reliability of the structure [38, 39]. Additional information regarding the amino acid sequence of the CYC target, pLDDT parameters, GMQE, and identity is available in the supporting information. In order to ensure structural fidelity, a model validation was performed. Hence, the 3D structure of the CYC protein was validated by the PROCHECK server (https://saves.mbi.ucla.edu/) [40, 41]. The Ramachandran plot reveals that 92.6% of the residues are located in the most favorable regions, 7.4% in the allowed regions, 0.0% in the generously disallowed regions, and 0.0% in the disallowed regions [40, 41] (Figure 1).

2.3 | Molecular Docking

Molecular docking is an approach that involves selecting lead compounds based on their affinity to targeted receptors [42]. The preparation of the two targets, CYC and RAS1, for molecular docking was done using ADT V. 1.5.7 by eliminating water

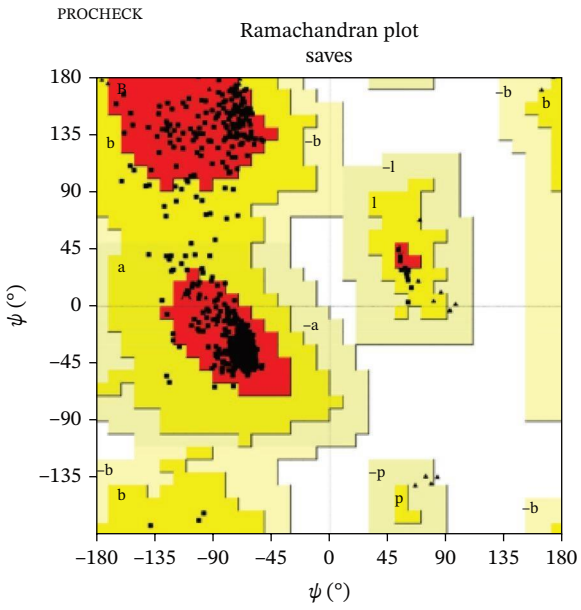


FIGURE 1 | Ramachandran plot of the protein CYC, displaying the distribution of each amino acid within the favored, allowed, and disallowed regions.

and heteroatoms and adding Kollman charges as well as polar hydrogens, and finally, the structures were saved in PDBQT format [33, 34]. Then, a blind docking was carried out by AutoDock Vina Version 1.2.5. First, a configuration file was created for the CYC (center_x = −1.426 Å, center_y = 12.486 Å, center_z = 2.103 Å; size_x = size_y = size_z = 90) and RAS1 (center_x = −20.842 Å, center_y = 33.067 Å, center_z = −19.399 Å; size_x = 58, size_y = 90, size_z = 84). The exhaustiveness parameter is set to 8, the number of binding modes to 10, and the energy range to a value of 4 kcal/mol. During the molecular docking process, the protein remains rigid and does not change conformation, whereas the ligand is flexible and adapts its conformation to optimize the binding with the protein [43]. The ligand–protein interactions were expressed in kilocalories per mole, with the complexes exhibiting the lowest binding energies being the strongest ones. Then, Lipinski's rules of the best compounds were assessed to predict their pharmacokinetic properties [44].

2.4 | Prediction of ADME-Tox Properties

The analysis of ADMET properties was carried out using a protocol of the ADMET descriptor algorithm pkCSM (https://biosig.lab.uq.edu.au/pkcsm/prediction). This web server helps us predict the parameters of absorption, distribution, metabolism, elimination, and toxicity [45]. The absorption of a drug requires the presence of several factors, namely, intestinal absorption, membrane permeability measured using Caco-2 (colon cancer cells), and skin permeability. The distribution of the drug candidate relies on factors such as the blood–brain barrier (BBB) (logBBB); then, metabolism is evaluated based on CYP2D6 and CYP3A4 models for the substrate as well as inhibition. Excretion is estimated based on the total clearance model, and finally, toxicity is focused on AMES toxicity, hERG I and II channel inhibition, and the maximum tolerated dose [45]. After verifying the ADME-toxicity properties, the ligands that met these criteria and exhibited the lowest binding energies were visualized using Discovery Studio Version 24.1.0.23298 and selected for molecular dynamic (MD) simulations.

2.5 | MM-GBSA Analysis

To validate the molecular docking protocol, the complexes were subjected to a generalized Born surface molecular mechanics (MM-GBSA) analysis to predict the binding free energy between a protein target and the ligand [46, 47]. This energy is calculated using the Prime MM-GBSA method integrated into Maestro of the Schrödinger suite by applying an OPLS3 force field [12, 48, 49]. The bond energy ΔG (bind) is calculated using the following formula:

$$\Delta G\,\text{bind} = \Delta G\,\text{coulomb} + \Delta G\,\text{covalent} + \Delta G\,\text{Hbond} + \Delta G\,\text{Lipo} + \Delta G\,\text{packing} + \Delta G\,\text{Solv GB} + \Delta G\,\text{VdW}.$$

2.6 | MD Simulations

MD simulations are of particular interest in modern in silico screening and are used to assess the stability of protein–ligand complexes over time [50–53]. These simulations consist of a representation of atomic movements over time, which provides information on the ligand's affinity for its target in a physiological environment by integrating Newton's equation [54, 55]. The MD simulations, lasting 100 ns, were performed using the Desmond software integrated into Schrödinger Maestro Version 2019-4. The protein–ligand complexes were solvated in a Transferable Intermolecular Potential 3-Point (TIP3P) water model within an orthorhombic simulation box [56]. The simulations were performed under physiological conditions, in an NPT ensemble (temperature = 300 K; pressure = 1 atm). An OPLS_2005 (Optimized Potentials for Liquid Simulations) force field was used to model the atoms in the system, and sodium chloride ions at a concentration of 0.15 M were added to maintain the neutrality of the system and simulate physiological conditions. Trajectory recordings were made every 100 ps [7, 50, 57].

2.7 | Three-Dimensional Superimposition of Protein Complexes and Structures

UCSF Chimera Version 1.19 is a molecular analysis and visualization software program used to overlay 3D structures of proteins and complexes [58, 59]. After extracting representative structures (proteins alone and complexes) in PDB format at (0 ns: initial image) and (100 ns: final image) based on the MD simulations trajectories, they were imported into Chimera to align the final structure (100 ns) with the reference structure (0 ns) using the Matchmaker tool. The proteins were distinguished by different colors, and the ligands were represented by molecular surfaces to highlight conformational changes.

3 | Results

C. albicans is the most commonly identified infectious yeast in humans. In the United States, this fungus is ranked among the Top 3 causes of bloodstream infections and the primary source of catheter-related infections, leading to a significant rate of colonization and death [60]. Today, QQ is considered a promising alternative following the failure or ineffectiveness of antifungals [61]. In the current study, a database of 48 phytochemicals was in silico screened by combining molecular docking and MD simulations to select the best ligands targeting QS receptors (CYC and RAS1) of *C. albicans*.

3.1 | Molecular Docking Screening

The QS mechanism in *C. albicans* is characterized by the continuous secretion of the natural ligand, farnesol, which binds to both CYC and RAS1 with a binding affinity of −7.0 kcal/mol. Furthermore, the most promising ligands, exhibiting binding affinities for the protein targets that are higher than those of the natural ligand, were selected. For the CYC receptor, chamazulene and γ-muurolene exhibited binding energies of −7.6 and −8.1 kcal/mol, respectively, with the CYC receptor. For the RAS1 receptor, chamazulene and γ-muurolene exhibited values of −7.1 kcal/mol.

3.2 | Molecular Interaction Studies

Analysis of interactions shows that, by binding to the CYC target, farnesol forms π-alkyl bonds with TYR 1292, ILE (1321 and 1325), and PRO (1324 and 1384) and a π-sigma bond only with TYR 1295 (Figure 2a,b). Chamazulene forms π-alkyl bonds with TYR (1292 and 1295), ILE 1321, and PRO 1384 (Figure 2c,d), while γ-muurolene forms π-alkyl bonds with VAL 286 and HIS 291 and π-sigma bonds with TYR (526 and 547) (Figure 2e,f). By binding to the RAS1 target, farnesol forms π-alkyl bonds with ARG 1207, LEU 1210, LYS 1211, VAL 1224, TYR 1225, and ILE 1258 and a conventional hydrogen bond with ARG 1264 (Figure 3a,b). Chamazulene forms a Van der Waals bond only with GLN 1246, a π-anion bond with GLU 1216, a π-sigma bond with ARG 1245, and π-alkyl bonds with PRO (1044 and 1217) (Figure 3c,d). Meanwhile, γ-muurolene forms mainly π-alkyl bonds with TYR (1206 and 1225), ARG 1207, LEU 1210, and VAL 1224 (Figure 3e,f). Based on the results of molecular docking and interaction analysis, we find that chamazulene and γ-muurolene bind effectively to protein targets by establishing mainly hydrophobic and electrostatic interactions.

3.3 | Free Energy Calculations

The total binding free energy ΔG binding (total) resulting from the interaction of ligands with CYC and RAS1 is shown in Table 1. γ-Muurolene forms the most stable complex, exhibiting binding free energies ΔG binding (total) of −74.87 and −58.61 kcal/mol, respectively, with the protein targets CYC and RAS1. This stability is due to strong lipophilic, Van der Waals, and coulombic interactions. In contrast, farnesol and chamazulene exhibit relatively low binding energies when binding to CYC and RAS1, respectively, with generally weak coulombic and Van der Waals contributions, indicating fewer stable interactions. Taken together, the results highlight the importance of coulombic and Van der Waals forces in the stability of the complexes.

3.4 | Prediction of ADME-Tox Properties

The results of the in silico prediction of the ADME-toxicity properties of the most promising ligands are shown in Table 2. The evaluation of physicochemical properties indicates that the compounds studied comply with Lipinski's rules, confirming their high oral bioavailability [62]. They have favorable skin permeability, with $\log K_p$ values exceeding −2.5 and an excellent intestinal absorption, greater than 30%, facilitating their absorption [37, 63]. The molecules studied have Caco-2 values below 8×10^{-6}, indicating their low permeability to Caco-2, while their logBBB values are greater than 0.3, indicating their ability to cross the BBB. It is essential to optimize their physicochemical properties in order to limit their penetration by increasing their molecular weight, provided that the molecular mass range is respected to ensure good

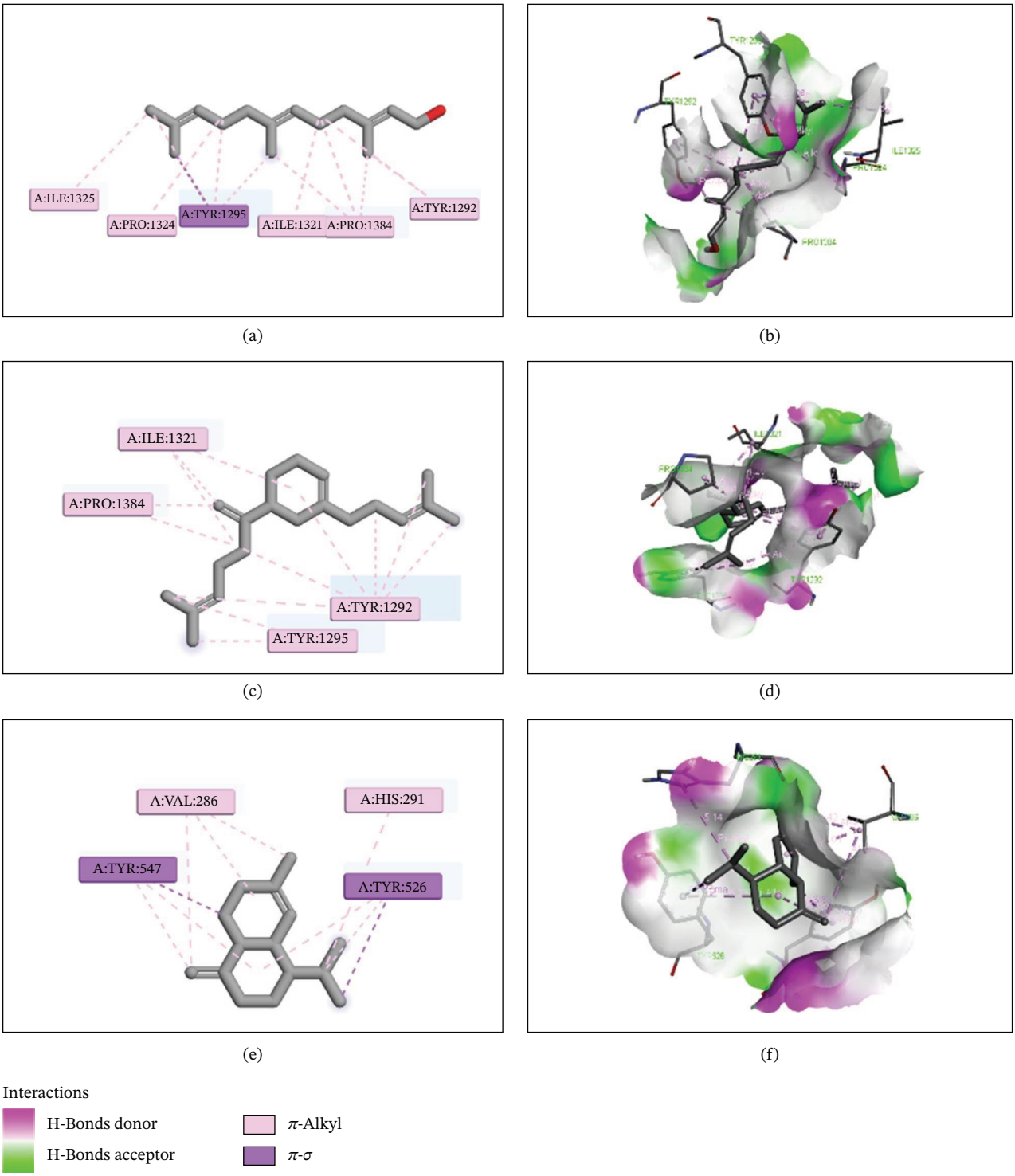


FIGURE 2 | Representation of protein–ligand interactions. (a) 2D visualization of interactions in the CYC-farnesol complex, (b) 3D visualization of interactions in the CYC-farnesol complex, (c) 2D visualization of interactions in the CYC-chamazulene complex, (d) 3D visualization of interactions in the CYC-chamazulene complex, (e) 2D visualization of interactions in the CYC-γ-muurolene complex, and (f) 3D visualization of interactions in the CYC-γ-muurolene complex.

oral absorption [64]. In contrast, molecules with a logBBB of less than −1 are expected to be poorly distributed in the brain [65, 66]. CYP3A4 and CYP2D6 are enzymes belonging to the cytochrome family, which play crucial roles in drug metabolism. However, none of the molecules is substrates or inhibitors of CYPs (3A4 and 2D6), indicating limited interaction with other drugs. The molecules are also not mutagenic (AMES), hepatotoxic, or inhibitors of hERG channels (I and II), meaning there is no risk of cardiac arrhythmias [67], except that chamazulene is relatively better tolerated than γ-muurolene due to its slightly higher dose compared to γ-muurolene. To sum up, chamazulene and γ-muurolene appear to be the most

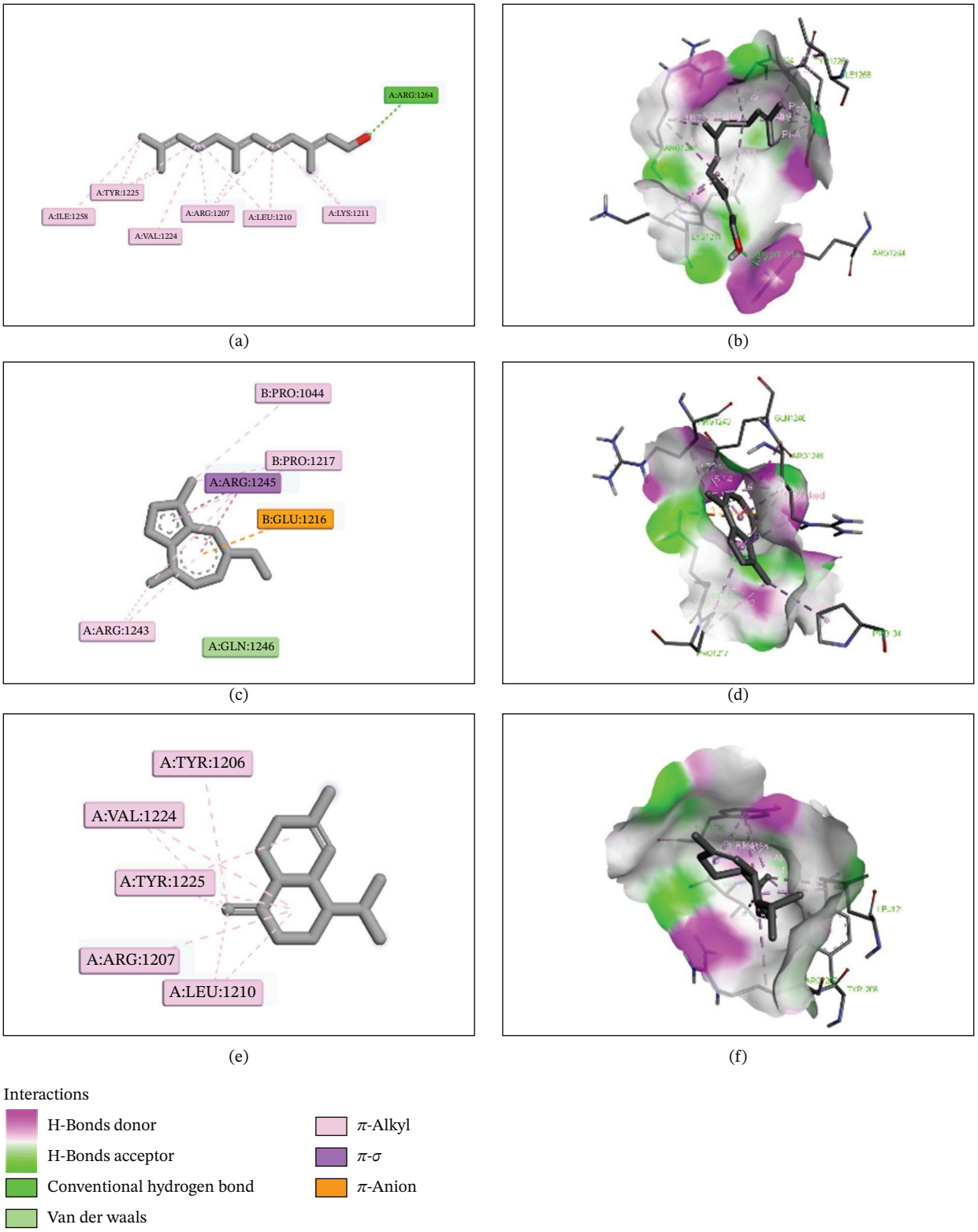


FIGURE 3 | Representation of protein–ligand interactions. (a) 2D visualization of interactions in the RAS1-farnesol complex, (b) 3D visualization of interactions in the RAS1-farnesol complex, (c) 2D visualization of interactions in the RAS1-chamazulene complex, (d) 3D visualization of interactions in the RAS1-chamazulene complex, (e) 2D visualization of interactions in the RAS1-γ-muurolene complex, and (f) 3D visualization of interactions in the RAS1-γ-muurolene complex.

TABLE 1 | MM-GBSA binding energy of the complex formed by farnesol, chamazulene, and γ-muurolene with the CYC and RAS1 receptors.

Complex	Δ *G* binding (total)	Δ *G*bind coulomb	Δ *G*bind Hbond	Δ *G*bind covalent	Δ *G*bindLipo	Δ *G*bind Solv GB	Δ *G*bind VdW	Δ *G*bind packing
CYC-farnesol	−66.00	−0.40	−0.06	−2.98	−43.68	15.58	−42.04	0.0
CYC-chamazulene	−61.73	−0.02	0	0.85	−44.75	10.41	−29.28	0.0
CYC-γ-muurolene	−74.87	−0.55	0	1.39	−52.93	13.51	−38.32	0.0
RAS1-farnesol	−49.47	−6.59	−0.23	3.02	−32.50	9.63	−24.52	0.0
RAS1-chamazulene	−44.09	−0.14	0	0.39	−29.11	3.54	−23.53	0.0
RAS1-γ-muurolene	−58.61	−0.67	0	1.35	−41.13	3.07	−28.99	0.0

Abbreviations: Hbond, hydrogen-bonding energy; Lipo, lipophilic energy; Solv GB, Born's generalized electrostatic solvation energy; VdW, Van der Waals energy.

TABLE 2 | In silico prediction of the ADME-Tox properties of chamazulene and γ-muurolene.

		Chamazulene	γ-Muurolene
Absorption and distribution	Skin permeability (log K_p)	−1.41	−1.561
	Intestinal absorption (human) (%)	94.503	96.475
	Caco-2 permeability (log Papp in 10−6 cm/s)	1.402	1.427
	LogBBB	0.792	0.809
Metabolism	CYP2D6/CYP3A4 substrate	No	No
	CYP2D6/CYP3A4 inhibitor	No	No
Excretion and toxicity	Total clearance (log ml/min/kg)	0.257	1.188
	AMES toxicity	No	No
	Max. tolerated dose (log mg/kg/day)	0.051	0.048
	hERG I/II inhibitor	No	No
	Hepatotoxicity	No	No

promising ligands due to their excellent ADMET properties, as well as their compliance with Lipinski's rules and, above all, their strong binding affinity with CYC and RAS1 proteins.

3.5 | MD Simulations

MD simulations allow the analysis of atomic movement within biomedical systems. It is used to predict the movement as well as the interaction of each atom over time (nanoseconds), with the longer the simulation time, the better. MD simulation helps us visualize ligand–protein interactions while explaining molecular interactions and their functional consequences [68]. In our study, we conducted a 100 ns MD simulation of chamazulene and γ-muurolene in complex with the CYC and RAS1 proteins. The entire set was then compared with the natural ligand, farnesol, based on parameters such as the root mean square deviation (RMSD), the root mean square fluctuation (RMSF), the secondary structure of the proteins, and the ligand–receptor interactions. From this comparison, we can understand the interactions and structural effects induced by the ligands on their targets. The RMSD plot measures the average conformational change in atomic positions and indicates whether the simulation is stable. While RMSF maps characterize the local changes of the entire protein chain throughout the MD simulation, indeed, if RMSF indicates a low value, it means that the region is rigid and characterized by stability, whereas if RMSF presents high values, it indicates that the regions are in motion [69].

3.5.1 | MD Simulations Analysis of CYC Receptor

3.5.1.1 | RMSD Analysis. For the CYC-farnesol complex, the protein backbone (Cα) shows an initial increase at the start of the simulation, indicating structural changes, and stabilizes around 13 Å (Figure 4a). After the ligand adjusts to the protein, RMSD reaches 4 Å in the first 20 ns, then stabilizes around 6 Å

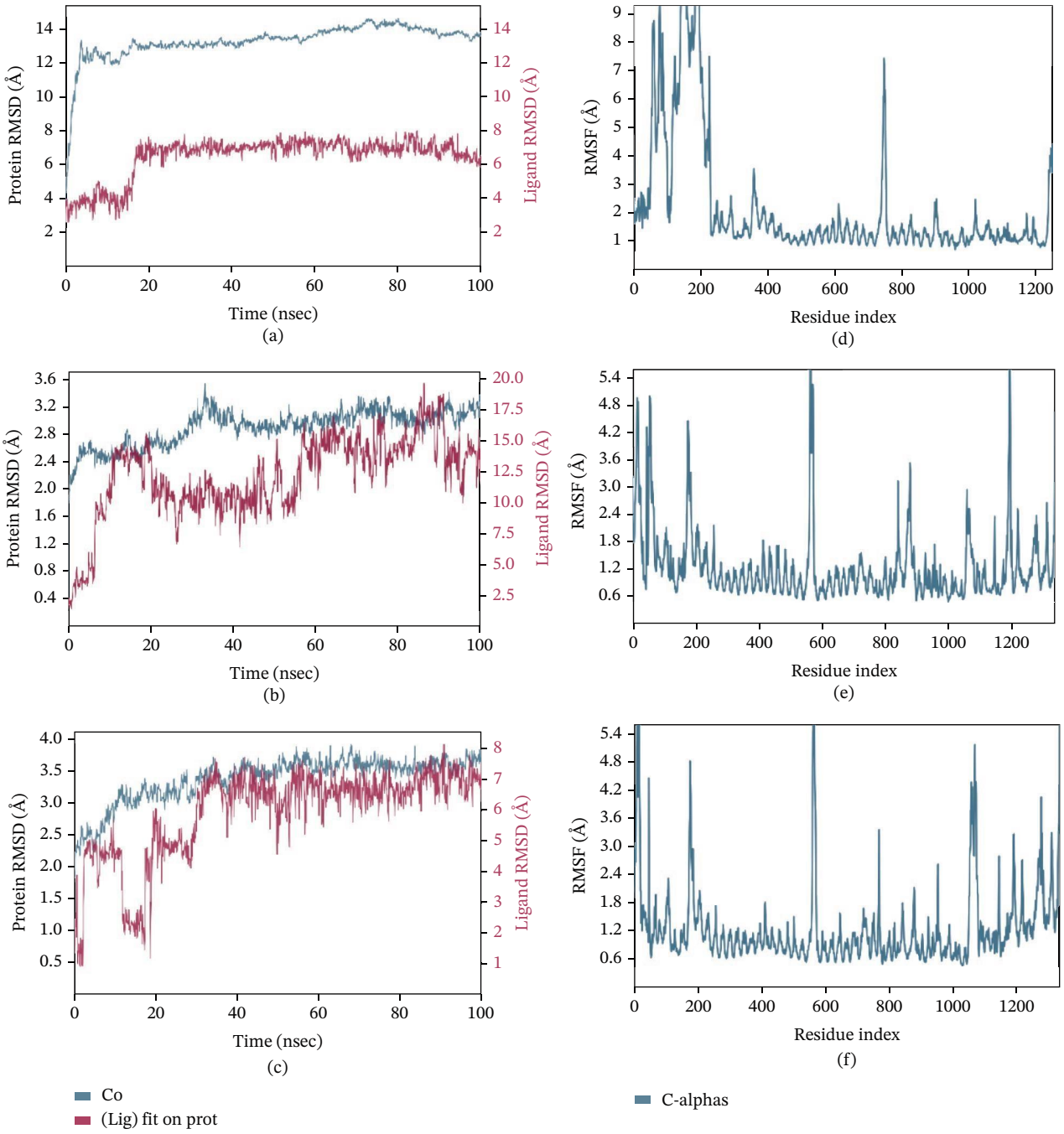


FIGURE 4 | Analysis of molecular dynamic simulation: (a) RMSD of the CYC-farnesol complex, (b) RMSD of the CYC-chamazulene complex, (c) RMSD of the CYC-γ-muurolene complex, (d) RMSF of the CYC-farnesol complex, (e) RMSF of the CYC-chamazulene complex, and (f) RMSF of the CYC-γ-muurolene complex.

during the rest of the simulation. For the CYC-chamazulene complex, at the start of the simulation, the RMSD of the protein increases to 2.6 Å, suggesting structural changes, then stabilizes between 2.8 and 3 Å during the rest of the simulation, with slight variations considered to be stable (Figure 4b). In contrast, the ligand undergoes pronounced fluctuations reaching 17.5 Å during the 100 ns of the simulation, suggesting a dynamic mode of interaction within the active site. For the CYC-γ-muurolene complex, in the first 10 ns, the RMSD of the protein gradually increases to around 2.8 Å and stabilizes at around 3 Å during the rest of the simulation, with small fluctuations suggesting a stable conformation (Figure 4c). In contrast, in the first 20 ns, the ligand exhibits moderate fluctuations, indicative of its conformational adaptation in the protein environment, from which point it exhibits fluctuations between 6.5 and 7.5 Å. Compared to farnesol, chamazulene and γ-muurolene are distinguished by their stability and conformational dynamics as the CYC-γ-muurolene complex stabilizes at a low RMSD (3 Å), while the CYC-farnesol complex varies around 13 Å. In addition, the RMSD of γ-muurolene reveals moderate conformational changes in the first 20 ns, with relative stabilization around 6.5 Å. Chamazulene, on the other hand, shows pronounced fluctuations reaching 17.5 Å, indicating significant conformational changes in the protein pocket. The results confirm the stability

of the γ-muurolene complex compared to farnesol and chamazulene complexes.

3.5.1.2 | RMSF Analysis. RMSF analysis is an important tool used to characterize the changes or local fluctuations of protein residues during the MD simulation trajectory and to distinguish the flexible parts from the stable parts of the protein [70]. In order to examine if the binding of potential drugs could be moved to another active site and if this is due to fluctuations [65], the CYC-farnesol complex exhibits high flexibility around residues located in the range of 2–200 and with an index of 750 (RMSF between 7 and 9 Å) (Figure 4d). Residues located in the regions 225–700 and 800–1200 are relatively stable, characterized by RMSF values below 4 Å. The CYC-chamazulene profile reveals that residues with indices of 75, 197, 500, 560, 850, 870, 1050, and 1200 exhibit significant fluctuations (2.4–5.4 Å) with the exception of residues in the range of 200–500, 600–800, and 900–1000, which show fluctuations of less than 2 Å (Figure 4e). In contrast, the RMSF profile of the CYC-γ-muurolene complex shows that most of the residues exhibit small fluctuations of less than 1.8 Å, indicating structural stability except for residues with indices 200, 550, 750, 950, 1050, and 1200, showing values between 2.4 and 5.4 Å (Figure 4f). RMSF analysis reveals that the CYC-γ-muurolene complex exhibits the greatest structural stability, with fluctuations of less than 1.8 Å for the majority of residues; chamazulene exhibits moderate stability (RMSF value less than 2 Å), while farnesol shows a less stable interaction (RMSF value less than 4 Å).

3.5.1.3 | Interaction Analysis and Contact Timeline. Regarding the CYC-farnesol complex (Figure 5a), ASN 517 represents the highest interaction percentage (0.6), mainly due to a hydrogen bond and a water bridge. TYR 634 (fraction 0.15) forms only a hydrophobic interaction, while ARG 77 (0.12) establishes a hydrogen bond, an ionic bond topped by a water bridge. The chronology of contacts in the CYC-farnesol complex is illustrated in Figure 5b which revealed that in the upper panel, the number of contacts varies between 1 and 2 and stabilizes after 20 ns, with ASN 517 and TYR 634 maintaining frequent contacts as shown in orange. For the CYC-chamazulene complex, ILE 1515 represents the highest fraction (over 0.25) by establishing only a hydrophobic interaction, while TRP 1438 (0.16), LEU 1487 (0.15), VAL 1483 (0.12), and PRO 1386 (0.10) establish the same type of interaction (Figure 5c). According to Figure 5d, the total number of contacts varies between 1 and 4 and stabilizes after 40 ns with ILE 1515, TRP 1438, LEU 1487, and VAL 1483 maintaining constant contacts (1–2) with strong interaction intensities represented in orange. For the CYC-γ-muurolene complex, TYR 547 represents the highest fraction (over 0.5) through a hydrophobic interaction in addition to both VAL 286 (fraction 0.25) and TYR 526 (0.17) (Figure 5e). According to Figure 5f, the total number of contacts varies between 2 and 4 and stabilizes after 25 ns, with TYR 547 and VAL 286 establishing regular contacts (1–3) with a high interaction intensity represented in orange throughout the simulation. Among the three ligands, γ-muurolene exhibits the most stable bond throughout the simulation due to high hydrophobic interactions that maintain the stability of the complex, compared to chamazulene and farnesol.

3.5.1.4 | Analysis of SSE. The percentage of secondary structure elements (SSEs) formed by farnesol with the CYC target is 24% (Figure 6a), whereas those of the two CYC-chamazulene complexes (Figure 6b) and CYC-γ-muurolene (Figure 6c) were considered at 30% and remained constant throughout the simulation. Indeed, the entire CYC structure remains stable when it binds to chamazulene and γ-muurolene, indicating the stability of both complexes.

3.5.2 | MD Simulation Analysis of RAS1 Receptor

3.5.2.1 | RMSD Analysis. For the RAS1-farnesol complex and during the first 60 ns, the RMSD values of both the protein and ligand show significant fluctuations, suggesting their conformational adaptation (Figure 7a). From this point onwards, the RMSD of RAS1 stabilizes relatively between 3.5 and 5.2 Å, while the RMSD of the ligand fluctuates between 6 and 7 Å. For the RAS1-chamazulene complex, the first 20 ns are characterized by a gradual increase in the RMSD profile to reach 12 Å, indicating a conformational adaptation, which then stabilizes relatively around 10.5 Å (Figure 7b). Similarly, in the first 20 ns, the ligand undergoes a rearrangement at the active site and then fluctuates between 4.5 and 9 Å during the rest of the simulation. For RAS1-γ-muurolene (Figure 7c), at the beginning, the RMSD of the protein and ligand increases with protein RMSD stabilizing between 1.75 and 2.5 Å in the first 40 ns, while that of the ligand stabilizes between 2.4 and 3.2 Å. Altogether, RMSD analysis reveals that the RAS1-γ-muurolene complex stabilizes at a low RMSD (1.75–2.5 Å), indicating that this complex is characterized by superior structural adaptation when bound to RAS1 compared to farnesol and chamazulene.

3.5.2.2 | RMSF Analysis. The RAS1-farnesol complex is characterized by significant flexibility, particularly around residues located in the ranges 125–175 and 400–425 and indices 200, 250, 300, 500, 600, 675, 700, and 775 (RMSF 3.2–5.6 Å) (Figure 7d). Residues located in the range 25–100 and indices 200, 225, 475, 625, and 800 show relative stability (RMSF less than 2.4 Å). For the RAS1-chamazulene complex, most residues are characterized by increased flexibility (3–8 Å), except for residues with indices 200, 275, 350, 375, 455, 550, and 600, showing RMSF values less than 2 Å (Figure 7e). In contrast, the RAS1-γ-muurolene complex is characterized by high structural stability as most fluctuations do not exceed 1.8 Å, except for residues 12, 75, 150, 175, and 338, which exceed 2.4 Å (Figure 7f). Hence, RMSF analysis reveals that the RAS1-γ-muurolene complex exhibits high overall stability, with the majority of residues fluctuating below 1.8 Å; however, chamazulene and farnesol exhibited fewer stable interactions.

3.5.2.3 | Interaction Analysis and Contact Timeline. For the RAS1-farnesol complex, GLU 895 represents the highest fraction percentage (0.33) that maintains the stability of the complex through hydrogen bonds, ionic bonds, and water bridges, while ASN 1271 (fraction 0.30) establishes a hydrogen bond topped by a water bridge (Figure 8a). PHE 1272 (0.18) forms a hydrophobic interaction, and GLY 1269 (0.17) forms a hydrogen bond and water bridge. Besides, THR 1268 (0.15) establishes a hydrogen bond and an ionic bond topped by a water bridge, while GLU 910 (0.175) forms a hydrogen bond, an ionic bond, and a water bridge. According to Figure 8b, the total number of contacts varies between

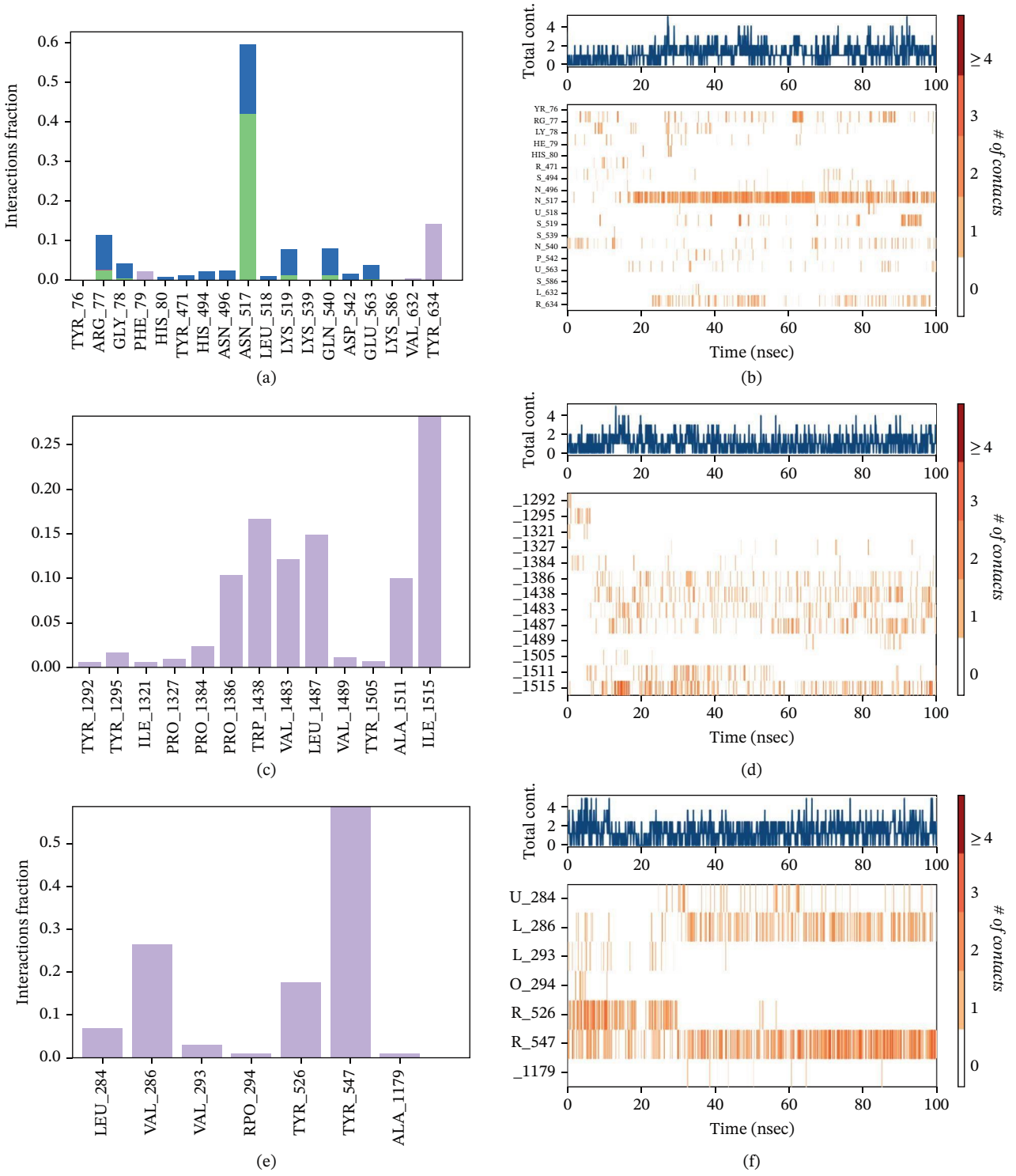


FIGURE 5 | Analysis of molecular dynamic simulation: (a) histogram of CYC-farnesol interactions, (b) CYC-farnesol contact timeline, (c) histogram of CYC-chamazulene interactions, (d) CYC-chamazulene contact timeline, (e) histogram of CYC-γ-muurolene interactions, and (f) CYC-γ-muurolene contact timeline.

1 and 3, with stabilization after 40 ns, with GLU 895 and PHE 1272 maintaining contacts over time. For the RAS1-chamazulene complex, PRO 1217 has the highest interaction percentage (0.40), forming a hydrophobic interaction in addition to PRO 1044 (with a fraction of 0.06) which forms the same type of interaction (Figure 8c). According to Figure 8d, the total number of contacts varies between 1 and 2, with PRO 1217 maintaining frequent contacts over time, as illustrated by a dark orange color. Regarding the RAS1-γ-muurolene complex, TYR 1225 has the highest fraction (over 0.30), mainly due to hydrophobic interactions in addition to LEU 1210 (0.26), VAL 1224 (0.16), and PHE 1265 (0.11) that established the same type of interaction (Figure 8e). According to Figure 8f, the total number of contacts varies between 2 and 4 and stabilizes during 60 ns, with TYR 1225 and PHE 1265 maintaining persistent contacts with a high interaction intensity represented in orange. Analysis of protein–ligand contacts reveals

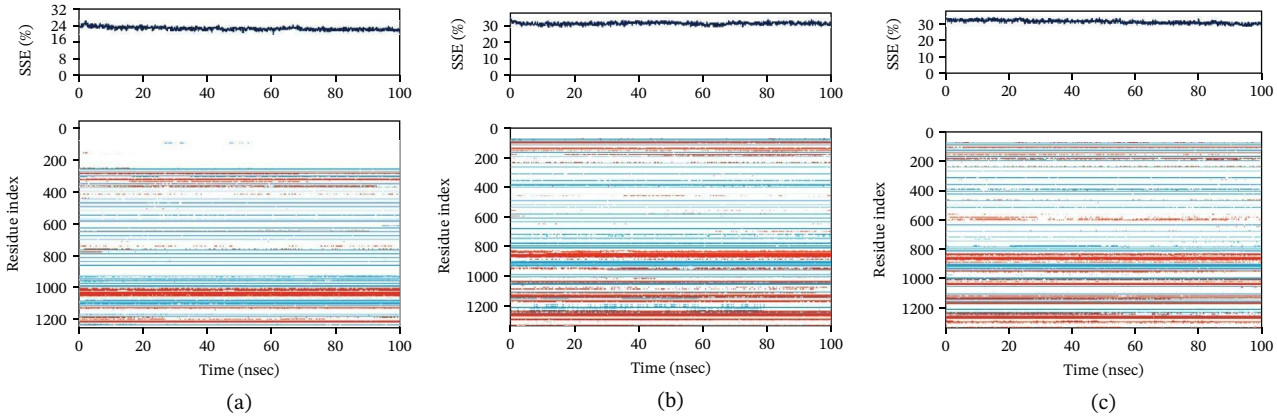


FIGURE 6 | (a) SSE map of CYC-farnesol complex, (b) SSE map of CYC-chamazulene complex, and (c) SSE map of CYC-γ-muurolene complex.

that γ-muurolene establishes stable bonds through high-fraction hydrophobic interactions, which make the interaction persistent and strong throughout the simulation, whereas farnesol and chamazulene are distinguished by moderate contacts.

3.5.2.4 | Analysis of SSE. The evaluation of changes in the SSE of RAS1 when it binds to each ligand over time revealed that the % SSE formed by farnesol with the RAS1 target was 58% (Figure 9a) and remained constant throughout the simulation. The same value and stability were observed in RAS1-chamazulene (Figure 9b) and RAS1-γ-muurolene (Figure 9c) complexes. Indeed, the entire RAS1 structure is stable when it binds to chamazulene and γ-muurolene, indicating a marked stability.

3.5.2.5 | Superimposition of Protein Complexes and Structures. To validate the MD simulation protocol, we assessed the structural stability of the proteins and complexes over the 100 ns simulation period by performing a 3D superimposition of the structures obtained at 0 and 100 ns. The conformations of the CYC proteins, shown in blue (0 ns) and red (100 ns) (Figure 10a), as well as the conformations of the RAS1 target shown in cyan (0 ns) and green (100 ns) (Figure 10d), demonstrated overall stability with minor variations in the flexible regions, suggesting slight conformational changes. By binding to CYC, chamazulene (Figure 10b) and γ-muurolene (Figure 10c) are firmly anchored at the active site, with limited displacements indicating slight conformational adjustments, exhibiting RMSD values of 1.191 and 1.252 Å, respectively. Similarly, upon binding to RAS1, chamazulene (Figure 10e) and γ-muurolene (Figure 10f) are anchored in the binding site with low RMSD values of 1.169 and 1.278 Å, respectively. Hence, the 0 and 100 ns superimposition analyses confirm the high structural stability of the CYC and RAS1 receptors in their free state and after complexation with both ligands. All RMSD values are less than 1.5 Å, indicating excellent structural stability of these complexes.

4 | Discussion

In our in silico investigation, we combined virtual screening with MD simulations to assess the potential of phytomolecules as inhibitors of QS receptors (CYC and RAS1) expressed in *C. albicans*. These molecules are derived from EOs extracted from three medicinal plants, *C. ladanifer*, *M. chamomilla*, and *P. lentiscus*, which have demonstrated marked anticandidal activity [30, 71]. QS inhibition is a highly effective therapeutic strategy for regulating the pathogenicity of *C. albicans* [7, 72], compared to the reference ligand, farnesol, which has been shown to be effective in inhibiting biofilm formation [60]. Virtual screening revealed that chamazulene (PubChem CDI: 10719) and γ-muurolene (PubChem CDI: 12313020) were among the most promising ligands, exhibiting the lowest binding energies, which are considered the best binding energies with the CYC protein target. While these differences in binding energy compared to the RAS1 target are relatively small (difference ~1 kcal/mol), this is due to the uncertainty inherent in the docking process. Regarding their interaction mechanisms, chamazulene and γ-muurolene exhibited a variety of hydrophobic, electrostatic, and Van der Waals interactions, in contrast to the reference ligand, which interacts primarily with proteins through hydrophobic contacts. These interactions maintain a strong and persistent bond and enhance the inhibitory activity of the ligands. To validate the molecular docking protocol and reduce docking uncertainty, MM-GBSA calculations revealed that γ-muurolene forms a stable complex with binding free energies of −74.87 and −58.61 kcal/mol with CYC and RAS1, respectively. This high stability is due to coulombic, lipophilic, and Van der Waals interactions, demonstrating that γ-muurolene is a promising QS inhibitor. Chamazulene establishes significant interactions but slightly weaker compared to γ-muurolene. Studies, such as those conducted by Jothi et al. [7], Shafiei et al. [73], and Simon et al. [74], have successfully combined in silico, in vitro, and in vivo approaches to identify QQMs with potential antifungal activity against *C. albicans* by targeting the same QS receptors. In fact, the experimental results corroborated the potential of the main compounds in silico. Indeed, virtual screening enables the effective identification of promising QQ molecules, and favorable in vitro results significantly increase the likelihood that these compounds will yield beneficial outcomes in subsequent experimental settings, thereby establishing a solid foundation for the continued development of drugs against *C. albicans*. The pkCSM server predicts that chamazulene and γ-muurolene have a favorable ADME-Tox profile and comply with Lipinski's rules, which confirms their oral bioavailability. They are characterized by excellent intestinal absorption, which facilitates their absorption following oral administration [37, 63]. These molecules can cross the BBB, and therefore, they can cause undesirable neurological effects and induce neurotoxicity [64]. To avoid these neurological complications, it is recommended to modify the physicochemical properties

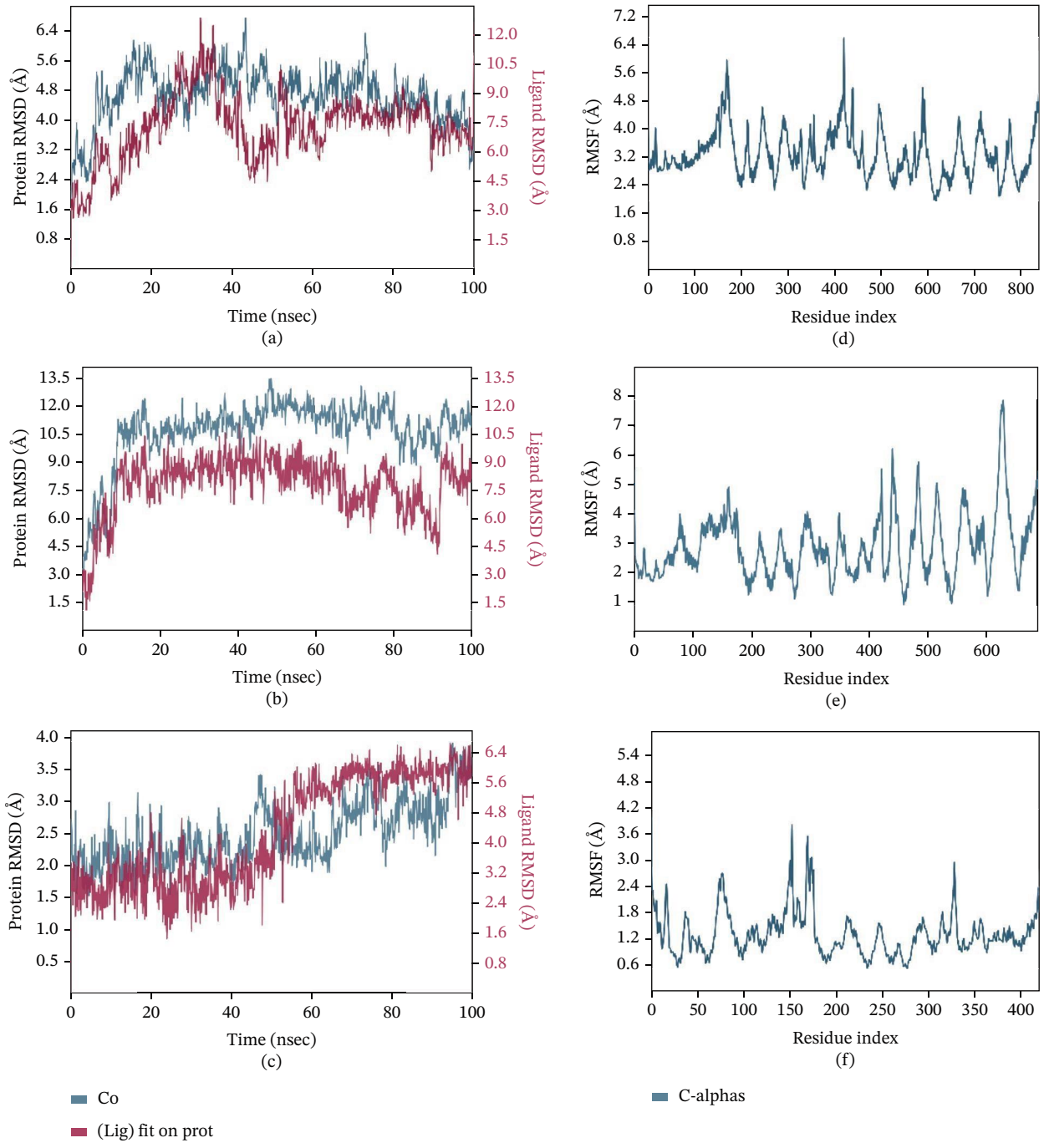


FIGURE 7 | Analysis of molecular dynamic simulation: (a) RMSD of the RAS1-farnesol complex, (b) RMSD of the RAS1-chamazulene complex, (c) RMSD of the RAS1-γ-muurolene complex, (d) RMSF of the RAS1-farnesol complex, (e) RMSF of the RAS1-chamazulene complex, and (f) RMSF of the RAS1-γ-muurolene complex.

of these molecules by setting a molecular weight between 450 and 500 kDa and a polar surface area between 70 and 140 Å^2 to preserve their excellent oral bioavailability and prevent their passage through the BBB [64]. On the contrary, in the case of cerebral fungal infections, the passage of these molecules through the BBB may be beneficial in treating them [75]. A recent study examined the antifungal effect of sulforaphane, a compound derived from cruciferous vegetables, against *C. albicans* and revealed that its ability to cross the BBB opens up new possibilities for the treatment of fungal infections affecting the central nervous system [55]. These two molecules do not interact with other drugs (neither substrates nor CYP enzyme inhibitors), and their toxicity profile is favorable as they exhibit no hepatic toxicity, no genetic mutations, and no impact on heart rate. Generally, both molecules are less well tolerated (dose below 0.477 log mg/kg/day), except that chamazulene is relatively better tolerated than γ-muurolene due to its slightly higher dose compared to γ-muurolene [76]. For MD simulations, analysis of the RMSD and RMSF allows for tracking the overall stability of the complexes and evaluating the flexibility of the residues, respectively [77, 78]. The number and type of interactions were tracked over the 100 ns of the simulation. The visualization of each protein residue's contacts with the ligand is

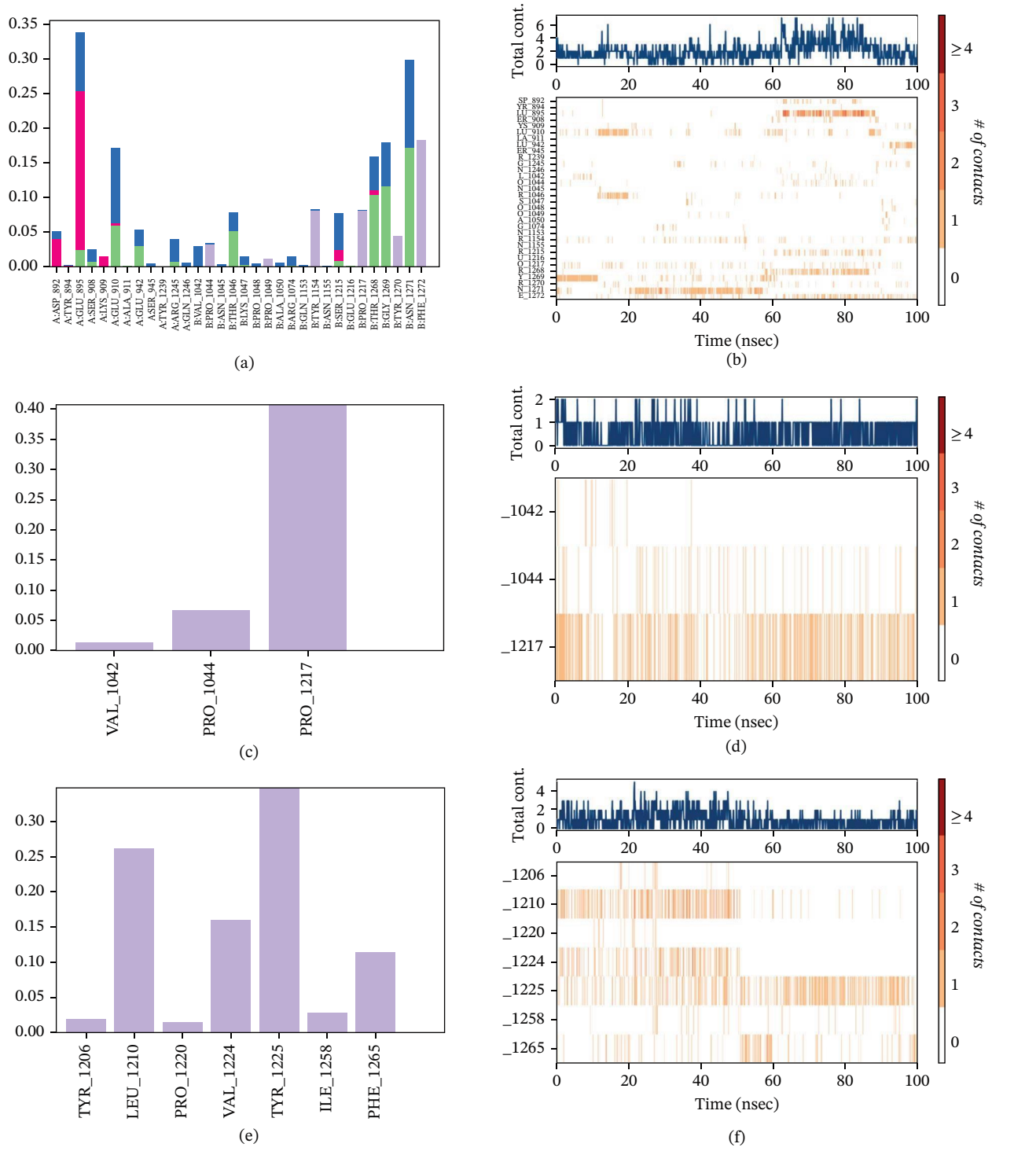


FIGURE 8 | Analysis of molecular dynamic simulation: (a) histogram of RAS1-farnesol interactions, (b) RAS1-farnesol contact timeline, (c) histogram of RAS1-chamazulene interactions, (d) RAS1-chamazulene contact timeline, (e) histogram of RAS1-γ-muurolene interactions, and (f) RAS1-γ-muurolene contact timeline.

determined by analyzing the timeline of interactions. Secondary structure element (SSE), a parameter that reveals the stability of protein secondary structures throughout the simulation [79]. The results confirm that γ-muurolene is the most promising ligand, exhibiting low RMSD values of 3 and 2.4 Å, respectively, with CYC and RAS1. This demonstrates its superior stability with these protein targets. RMSF analysis reveals that the complexes formed by γ-muurolene are distinguished by greater structural stability, as demonstrated by low fluctuations (generally less than 1.8 Å) for the majority of protein residues. This stability is maintained primarily through significant hydrophobic interactions throughout the simulation, particularly with the amino acids TYR (547 and 526) and VAL 286 at the CYC site and TYR 1225, LEU 1210, VAL 1224, and PHE 1265 at the RAS1 active site. This stability was confirmed by analysis of the SSE, which shows that the binding of γ-muurolene does not affect protein stability. This is consistent

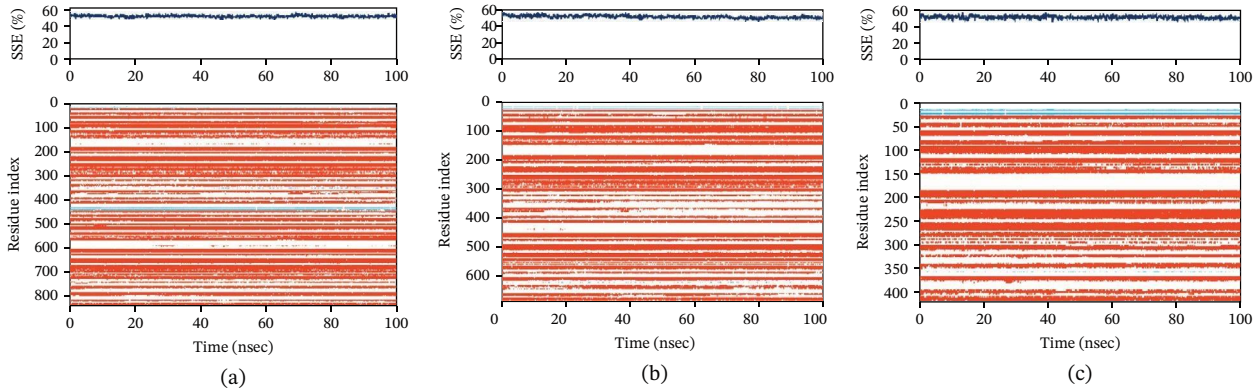


FIGURE 9 | (a) SSE map of RAS1-farnesol complex, (b) SSE map of RAS1-chamazulene complex, and (c) SSE map of RAS1-γ-muurolene complex.

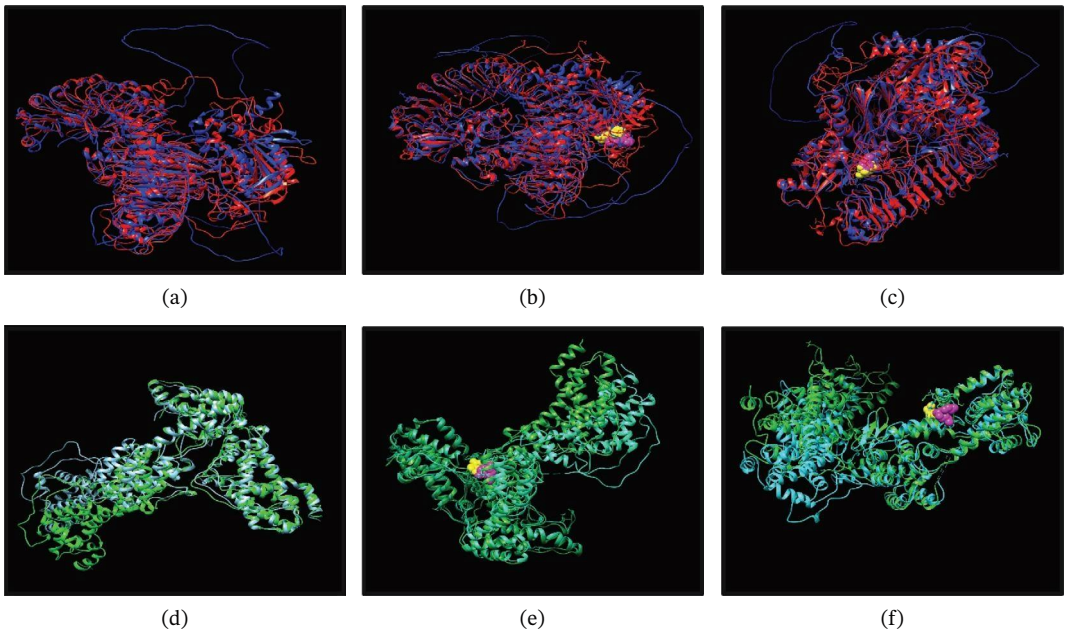


FIGURE 10 | Superimposition of the 3D structures of proteins and protein–ligand complexes at the initial (0 ns) and final (100 ns) time points of the MD simulation. (a) 3D superimposition of the CYC protein, (b) 3D superimposition of CYC and chamazulene, (c) 3D superimposition of CYC and γ-muurolene, (d) 3D superimposition of the RAS1 protein, (e) 3D superimposition of RAS1 and chamazulene, and (f) 3D superimposition of RAS1 and γ-muurolene.

with the screening results showing that γ-muurolene exhibits a notable and significant affinity compared to chamazulene and farnesol, which showed high RMSD values, suggesting conformational adaptations by binding to protein active sites. They exhibit fewer stable interactions with most protein residues. Furthermore, their RMSF profiles reveal that farnesol and chamazulene are characterized by moderate contacts during the simulation. To validate the reliability of the MD simulation, a 3D superimposition of the proteins and their complexes over a 100 ns confirmed the conformational stability of the CYC and RAS1 proteins, showing near-perfect alignment (RMSD < 1.19 Å). By binding to CYC, chamazulene and γ-muurolene remain attached to the active binding site and retain their initial conformations obtained by docking, with slight conformational adjustments, for which the RMSD values are 1.191 and 1.252 Å, respectively. Similarly, by binding to RAS1, chamazulene and γ-muurolene are fixed in the binding site with low RMSD values of 1.169 and 1.278 Å, respectively, confirming excellent structural stability of the CYC and RAS1 protein targets in the free state and after complexation with the ligands. To contextualize our results, in vitro studies show that γ-muurolene accounts for 16.6% of the EO of *Schinus terebinthifolius* Raddi and that its combination with conventional antibiotics enhances its antibiotic and antibacterial activity against *Escherichia coli*, *Pseudomonas aeruginosa*, and *Staphylococcus aureus* [80]. Another study highlighted the anticancer, anti-inflammatory, and antioxidant properties of *Garcinia intermedia* leaf extracts, one of whose sesquiterpene compounds is γ-muurolene [81]. Other studies have shown that γ-muurolene is one of the bioactive compounds present in the n-hexane fraction of the Indonesian medicinal plant *Typhonium flagelliforme* and is responsible for its strong antioxidant and anticancer potential [82]. A computational study suggests that γ-muurolene is one of the sesquiterpenes in the plant *Chrysopogon zizanioides*, known as Ramacham, that is responsible for several biological activities, including antibacterial activity [83]. Meanwhile, other studies have demonstrated the antifungal effect of chamazulene based on in vitro tests. Chamazulene was among the main compounds in *Artemisia* EOs and is responsible for the antifungal activity

against *Fusarium culmorum* [84]. Another study shows that the presence of high levels of chamazulene in yarrow EOs confers bactericidal, anti-inflammatory, wound-healing, and antiallergic effects. The study also highlights the sensitivity of chamazulene to strains of *C. albicans*, particularly *S. aureus* (MRSA) [85]. Antimicrobial activity tests on the EO of *Achillea asplenifolia* Vent. revealed significant bactericidal and fungicidal effects against *C. albicans*, respectively. This is due to the chemical composition of the oil, in which chamazulene serves as the major component, accounting for 25.6% [66]. In addition to its antibiofilm role, chamazulene confers a high antioxidant effect on chamomile EOs, as demonstrated following its extraction by column chromatography, since this bioactive molecule exhibited high antioxidant activity ($IC_{50} = 6.4\ \mu g\,mL^{-1}$) compared to other constituents of chamomile oils [86]. Furthermore, in addition to its inhibitory effect on biofilm formation by *C. albicans*, a study by Mathlouthi and his team shows that chamazulene is one of the most abundant compounds in the plants *Artemisia herba-alba*, *Artemisia campestris*, and *Artemisia absinthium* and that it inhibits biofilm formation in *E. coli* without affecting cell growth [87]. Our results reveal that γ-muurolene is a potential inhibitor of QS in *C. albicans* and can be used to inhibit biofilm formation. However, our in silico studies necessarily require experimental studies to confirm the predicted results, and future research must include cytotoxicity, biochemical assays, animal models, and an in-depth investigation of the signaling pathways modulated by γ-muurolene.

5 | Conclusion

The present study has enabled us to tackle a major challenge, namely, the formation of biofilms by *C. albicans*. The problem lies in the fact that this yeast develops increased resistance to antifungal agents. Virtual screening of 48 molecules followed by MD simulations led to the selection of γ-muurolene as a potential inhibitor of two QS receptors expressed by *C. albicans*. The ability of this molecule to inhibit QS in *C. albicans* needs to be complemented by extensive experimental studies.

Author Contributions

Conceptualization: Doha EL Meskini, Fettouma Chraa, Taoufiq Benali, and Tarik Aanniz; methodology: Doha EL Meskini, Fettouma Chraa, Taoufiq Benali, Abdelhakim Bouyahya, and Tarik Aanniz; validation: Hooi Leng Ser, Bey Hing Goh, Rachid El Jaoudi, and Mouna Ouadghiri: writing—original draft preparation: Doha EL Meskini, Bey Hing Goh, and Tarik Aanniz; writing—review and editing: Doha EL Meskini, Hooi Leng Ser, and Tarik Aanniz; supervision and project administration: Abdelhakim Bouyahya, Tarik Aanniz, Hooi Leng Ser, and Bey Hing Goh.

Acknowledgments

Doha EL Meskini and Fettouma Chraa gratefully acknowledge the support of the CNRST (National Center for Scientific and Technical Research), Morocco, as part of the PhD-Associate Scholarship Program (PASS).

Funding

No funding was received for this manuscript. Open access publishing facilitated by University of Technology Sydney, as part of the Wiley - University of Technology Sydney agreement via the Council of Australasian University Librarians.

Conflicts of Interest

The authors declare no conflicts of interest.

Data Availability Statement

The data that support the findings of this study are available from the corresponding authors upon reasonable request.

References

1. J. R. Naglik, S. L. Gaffen, and B. Hube, "Candidalysin: Discovery and Function in Candida Albicans Infections," *Current Opinion in Microbiology* 52 (2019): 100–109, https://doi.org/10.1016/j.mib.2019.06.002.

2. M. Kruppa, "Quorum Sensing and Candida Albicans," *Mycoses* 52, no. 1 (2009): 1–10, https://doi.org/10.1111/j.1439-0507.2008.01626.x.

3. E. Paramonova, B. P. Krom, H. C. van der Mei, H. J. Busscher, and P. K. Sharma, "Hyphal Content Determines the Compression Strength of Candida albicans Biofilms," *Microbiology* 155, no. 6 (2009): 1997–2003, https://doi.org/10.1099/mic.0.021568-0.

4. C. Tsui, E. F. Kong, and M. A. Jabra-Rizk, "Pathogenesis of Candida albicans Biofilm," *FEMS Pathogens and Disease* 74, no. 4 (2016): ftw018, https://doi.org/10.1093/femspd/ftw018.

5. R. Pereira, R. O. Santos Fontenelle, E. H. S. Brito, and S. M. Morais, "Biofilm of Candida Albicans: Formation, Regulation and Resistance," *Journal of Applied Microbiology* 131, no. 1 (2021): 11–22, https://doi.org/10.1111/jam.14949.

6. M. Polke, I. Leonhardt, O. Kurzai, and I. D. Jacobsen, "Farnesol Signalling in Candida albicans - More Than Just Communication," *Critical Reviews in Microbiology* 44, no. 2 (2018): 230–243, https://doi.org/10.1080/1040841X.2017.1337711.

7. R. Jothi, N. Hari Prasath, S. Gowrishankar, and S. K. Pandian, "Bacterial Quorum-Sensing Molecules as Promising Natural Inhibitors of Candida albicans Virulence Dimorphism: An In Silico and In Vitro Study," *Frontiers in Cellular and Infection Microbiology* 11 (2021): 781790, https://doi.org/10.3389/fcimb.2021.781790.

8. A. Davis-Hanna, A. E. Piispanen, L. I. Stateva, and D. A. Hogan, "Farnesol and Dodecanol Effects on the Candida albicans RAS1-cAMP Signalling Pathway and the Regulation of Morphogenesis," *Molecular Microbiology* 67, no. 1 (2008): 47–62, https://doi.org/10.1111/j.1365-2958.2007.06013.x.

9. A. Deveau, A. E. Piispanen, A. A. Jackson, and D. A. Hogan, "Farnesol Induces Hydrogen Peroxide Resistance in Candida albicans Yeast by Inhibiting the RAS-Cyclic AMP Signaling Pathway," *Eukaryotic Cell* 9, no. 4 (2010): 569–577, https://doi.org/10.1128/EC.00321-09.

10. T. L. Han, R. D. Cannon, and S. G. Villas-Bôas, "The Metabolic Basis of Candida albicans Morphogenesis and Quorum Sensing," *Fungal Genetics and Biology* 48, no. 8 (2011): 747–763, https://doi.org/10.1016/j.fgb.2011.04.002.

11. A. Mehmood, G. Liu, X. Wang, G. Meng, C. Wang, and Y. Liu, "Fungal Quorum-Sensing Molecules and Inhibitors With Potential Antifungal Activity: A Review," *Molecules* 24, no. 10 (2019): 1950, https://doi.org/10.3390/molecules24101950.

12. F. Chraa, D. El Meskini, I. Kandoussi, et al., "Exploring Propolis-Derived Compounds as Quorum Sensing Inhibitors for Candida

albicans: A Molecular Docking and Dynamics Simulations Study," *Scientific Reports* 15, no. 1 (2025): 32899, https://doi.org/10.1038/s41598-025-18001-1.

13. F. Hemmati, R. Salehi, R. Ghotaslou, et al., "Quorum Quenching: A Potential Target for Antipseudomonal Therapy," *Infection and Drug Resistance* 13 (2020): 2989–3005, https://doi.org/10.2147/IDR.S263196.

14. C. Spaggiari, C. Yamukujije, M. Pieroni, and G. Annunziato, "Quorum Sensing Inhibitors (QSIs): A Patent Review (2019-2023)," *Expert Opinion on Therapeutic Patents* 35 (2025): 657–673, https://doi.org/10.1080/13543776.2025.2491382.

15. A. M. Pereira, B. F. da Silva, I. M. Araujo, et al., "Antibacterial and Antibiofilm Activities of Hydralazine, an Antihypertensive Drug: In Vitro and In Silico Approaches," *Antibiotics* 14, no. 3 (2025): 286, https://doi.org/10.3390/antibiotics14030286.

16. A. A. Abdelaziz, A. M. Abo-Kamar, A. E. Ashour, M. A. Shaldam, and E. Elekhnawy, "Unveiling the Antibacterial Action of Ambroxol Against Staphylococcus aureus Bacteria: In Vitro, In Vivo, and In Silico Investigation," *BMC Microbiology* 24, no. 1 (2024): 507, https://doi.org/10.1186/s12866-024-03666-x.

17. J. Chadha, L. Khullar, P. Gulati, S. Chhibber, and K. Harjai, "Repurposing Albendazole as a Potent Inhibitor of Quorum Sensing-Regulated Virulence Factors in Pseudomonas aeruginosa: Novel Prospects of a Classical Drug," *Microbial Pathogenesis* 186 (2024): 106468, https://doi.org/10.1016/j.micpath.2023.106468.

18. Y. Yuan, X. Yang, Q. Zeng, et al., "Repurposing Dimetridazole and Ribavirin to Disarm Pseudomonas aeruginosa Virulence by Targeting the Quorum Sensing System," *Frontiers in Microbiology* 13 (2022): 978502, https://doi.org/10.3389/fmicb.2022.978502.

19. D. Liu, Y. Lu, Z. Li, X. Pang, and X. Gao, "Quorum Sensing: Not Just a Bridge Between Bacteria," *MicrobiologyOpen* 14, no. 1 (2025): e70016, https://doi.org/10.1002/mbo3.70016.

20. I. S. Bayer, "Fungal Quorum Sensing Molecules as Potential Drugs in the Treatment of Chronic Wounds and Their Delivery," *Expert Opinion on Drug Delivery* 22, no. 2 (2025): 277–296, https://doi.org/10.1080/17425247.2025.2452303.

21. S. Liu, X. Feng, H. Zhang, P. Li, B. Yang, and Q. Gu, "Decoding Bacterial Communication: Intracellular Signal Transduction, Quorum Sensing, and Cross-Kingdom Interactions," *Microbiological Research* 292 (2025): 127995, https://doi.org/10.1016/j.micres.2024.127995.

22. X. Liu, J. Luo, Q. Xu, Q. Lu, B. J. Ni, and D. Wang, "Roles and Opportunities of Quorum Sensing in Natural and Engineered Anaerobic Digestion Systems," *Water Research* 275 (2025): 123190, https://doi.org/10.1016/j.watres.2025.123190.

23. Â. Luís, and F. Domingues, "Quorum Sensing Inhibition Evaluation Method: An Experiment-Based Microbiology Laboratory Course," *Biochemistry and Molecular Biology Education* 53, no. 2 (2025): 191–199, https://doi.org/10.1002/bmb.21874.

24. S. Fetzner, "Quorum Quenching Enzymes," *Journal of Biotechnology* 201 (2015): 2–14, https://doi.org/10.1016/j.jbiotec.2014.09.001.

25. S. Mion, B. Rémy, L. Plener, É. Chabrière, and D. Daudé, "Quorum sensing et quorum quenching: Comment bloquer la communication des bactéries pour inhiber leur virulence?," *Médecine/Sciences* 35, no. 1 (2019): 31–38, https://doi.org/10.1051/medsci/2018310.

26. J. Park, R. Jagasia, G. F. Kaufmann, et al., "Infection Control by Antibody Disruption of Bacterial Quorum Sensing Signaling," *Chemistry & Biology* 14, no. 10 (2007): 1119–1127, https://doi.org/10.1016/j.chembiol.2007.08.013.

27. N. Kato, T. Morohoshi, T. Nozawa, H. Matsumoto, and T. Ikeda, "Control of Gram-Negative Bacterial Quorum Sensing With Cyclodextrin Immobilized Cellulose Ether Gel," *Journal of Inclusion Phenomena and Macrocyclic Chemistry* 56, no. 1-2 (2006): 55–59, https://doi.org/10.1007/s10847-006-9060-y.

28. S. Scutera, M. Zucca, and D. Savoia, "Novel Approaches for the Design and Discovery of Quorum-Sensing Inhibitors," *Expert Opinion on Drug Discovery* 9, no. 4 (2014): 353–366, https://doi.org/10.1517/17460441.2014.894974.

29. K. Tang, and X. H. Zhang, "Quorum Quenching Agents: Resources for Antivirulence Therapy," *Marine Drugs* 12, no. 6 (2014): 3245–3282, https://doi.org/10.3390/md12063245.

30. T. Benali, M. Laghmari, J. Touhtouh, et al., "Chemical Composition and Bioactivity of Essential Oils From Cistus ladanifer L., Pistacia lentiscus L., and Matricaria chamomilla L," *Biochemical Systematics and Ecology* 116 (2024): 104880, https://doi.org/10.1016/j.bse.2024.104880.

31. S. Kim, "Getting the Most Out of PubChem for Virtual Screening," *Expert Opinion on Drug Discovery* 11, no. 9 (2016): 843–855, https://doi.org/10.1080/17460441.2016.1216967.

32. Y. Wang, S. H. Bryant, T. Cheng, et al., "PubChem BioAssay: 2017 Update," *Nucleic Acids Research* 45, no. D1 (2017): D955–D963, https://doi.org/10.1093/nar/gkw1118.

33. J. Touhtouh, M. Laghmari, T. Benali, et al., "Determination of the Antioxidant and Enzyme-Inhibiting Activities and Evaluation of Selected Terpenes' ADMET Properties: In Vitro and In Silico Approaches," *Biochemical Systematics and Ecology* 111 (2023): 104733, https://doi.org/10.1016/j.bse.2023.104733.

34. J. Touhtouh, M. Laghmari, T. Benali, et al., "Evaluation of Antioxidant, Antimicrobial, Antidiabetic, Anti-Tyrosinase, and Neuroprotective Effects of β-Ionone: In Vitro and In Silico Analysis," *Results in Chemistry* 12 (2024): 101874, https://doi.org/10.1016/j.rechem.2024.101874.

35. J. Jumper, R. Evans, A. Pritzel, et al., "Highly Accurate Protein Structure Prediction With AlphaFold," *Nature* 596, no. 7873 (2021): 583–589, https://doi.org/10.1038/s41586-021-03819-2.

36. V. Mariani, M. Biasini, A. Barbato, and T. Schwede, "lDDT: A Local Superposition-Free Score for Comparing Protein Structures and Models Using Distance Difference Tests," *Bioinformatics* 29, no. 21 (2013): 2722–2728, https://doi.org/10.1093/bioinformatics/btt473.

37. D. El Meskini, F. Chraa, J. Touhtouh, et al., "Chrysin and Luteolin From Moroccan Propolis to Prevent Aggressive Periodontitis Caused by Aggregatibacter actinomycetemcomitans Leukotoxin: A Computer-Aided Drug Design Approach," *Pharmaceuticals* 19, no. 1 (2026): 115, https://doi.org/10.3390/ph19010115.

38. M. Biasini, S. Bienert, A. Waterhouse, et al., "SWISS-MODEL: Modelling Protein Tertiary and Quaternary Structure Using Evolutionary Information," *Nucleic Acids Research* 42, no. W1 (2014): W252–W258, https://doi.org/10.1093/nar/gku340.

39. A. Waterhouse, M. Bertoni, S. Bienert, et al., "SWISS-MODEL: Homology Modelling of Protein Structures and Complexes," *Nucleic Acids Research* 46, no. W1 (2018): W296–W303, https://doi.org/10.1093/nar/gky427.

40. Y. Boulaamane, M. Panadero, A. Hmadcha, et al., "Antibiotic Discovery With Artificial Intelligence for the Treatment of Acinetobacter baumannii Infections," *Msystems* 9, no. 6 (2024): e00325-24, https://doi.org/10.1128/msystems.00325-24.

41. M. Yousuf, K. Mammadova, M. Phil, L. Khan, and M. Phil, "Homology Modeling of α- Glucosidase Enzyme: 3D Structure Prediction," *Bioinformatics Review* 4, no. 11 (2018): .

42. J. Fan, A. Fu, and L. Zhang, "Progress in Molecular Docking," *Quantitative Biology* 7, no. 2 (2019): 83–89, https://doi.org/10.1007/s40484-019-0172-y.

43. N. T. Nguyen, T. H. Nguyen, T. N. H. Pham, et al., "AutoDock Vina Adopts More Accurate Binding Poses but AutoDock4 Forms Better

Binding Affinity," *Journal of Chemical Information and Modeling* 60, no. 1 (2020): 204–211, https://doi.org/10.1021/acs.jcim.9b00778.

44. C. A. Lipinski, F. Lombardo, B. W. Dominy, and P. J. Feeney, "Experimental and Computational Approaches to Estimate Solubility and Permeability in Drug Discovery and Development Settings," *Advanced Drug Delivery Reviews* 46, no. 1-3 (2001): 3–26, https://doi.org/10.1016/s0169-409x(00)00129-0.

45. P. Kavaliauskas, B. Grybaite, V. Mickevicius, et al., "Synthesis, ADMET Properties, and In Vitro Antimicrobial and Antibiofilm Activity of 5-Nitro-2-Thiophenecarbaldehyde N-((E)-(5-Nitrothienyl) Methylidene)Hydrazone (KTU-286) Against Staphylococcus aureus With Defined Resistance Mechanisms," *Antibiotics* 9, no. 9 (2020): 612, https://doi.org/10.3390/antibiotics9090612.

46. S. Gudipati, R. Muttineni, A. U. Mankad, H. A. Pandya, and Y. T. Jasrai, "Molecular Docking Based Screening of Noggin Inhibitors," *Bioinformation* 14, no. 1 (2018): 015–020, https://doi.org/10.6026/97320630014015.

47. P. Vediappan, M. Arumugam, and R. Natarajan, "In-Silico Design, ADMET Screening, Prime MM-GBSA Binding Free Energy Calculation and MD Simulation of Some Novel Phenothiazines as 5HT6R Antagonists Targeting Alzheimer's Disease," *Current Computer-Aided Drug Design* 21, no. 4 (2025): 487–502, https://doi.org/10.2174/0115734099282836231212064925.

48. S. Genheden, and U. Ryde, "The MM/PBSA and MM/GBSA Methods to Estimate Ligand-Binding Affinities," *Expert Opinion on Drug Discovery* 10, no. 5 (2015): 449–461, https://doi.org/10.1517/17460441.2015.1032936.

49. J. Kim, H. Jin, J. Kim, et al., "Leveraging the Fragment Molecular Orbital and MM-GBSA Methods in Virtual Screening for the Discovery of Novel Non-Covalent Inhibitors Targeting the TEAD Lipid Binding Pocket," *International Journal of Molecular Sciences* 25, no. 10 (2024): 5358, https://doi.org/10.3390/ijms25105358.

50. R. K. Mohapatra, A. Mahal, A. Ansari, et al., "Comparison of the Binding Energies of Approved Mpox Drugs and Phytochemicals Through Molecular Docking, Molecular Dynamics Simulation, and ADMET Studies: An In Silico Approach," *Journal of Biosafety and Biosecurity* 5, no. 3 (2023): 118–132, https://doi.org/10.1016/j.jobb.2023.09.001.

51. P.-C. Do, E. H. Lee, and L. Le, "Steered Molecular Dynamics Simulation in Rational Drug Design," *Journal of Chemical information and Modeling* 58, no. 8 (2018): 1473–1482, https://doi.org/10.1021/acs.jcim.8b00261.

52. L. Liu, Y. Jiao, M. Yang, L. Wu, G. Long, and W. Hu, "Network Pharmacology, Molecular Docking and Molecular Dynamics to Explore the Potential Immunomodulatory Mechanisms of Deer Antler," *International Journal of Molecular Sciences* 24, no. 12 (2023): 10370, https://doi.org/10.3390/ijms241210370.

53. X. Wu, L. Y. Xu, E. M. Li, and G. Dong, "Application of Molecular Dynamics Simulation in Biomedicine," *Chemical Biology & Drug Design* 99, no. 5 (2022): 789–800, https://doi.org/10.1111/cbdd.14038.

54. P. W. Hildebrand, A. S. Rose, and J. K. S. Tiemann, "Bringing Molecular Dynamics Simulation Data Into View," *Trends in Biochemical Sciences* 44, no. 11 (2019): 902–913, https://doi.org/10.1016/j.tibs.2019.06.004.

55. B. L. Silva, G. Simão, C. D. Campos, et al., "In Silico and In Vitro Analysis of Sulforaphane Anti-Candida Activity," *Antibiotics* 11, no. 12 (2022): 1842, https://doi.org/10.3390/antibiotics11121842.

56. L. Ivanova, J. Tammiku-Taul, A. T. García-Sosa, Y. Sidorova, M. Saarma, and M. Karelson, "Molecular Dynamics Simulations of the Interactions Between Glial Cell Line-Derived Neurotrophic Factor Family Receptor GFRα1 and Small-Molecule Ligands," *ACS Omega* 3, no. 9 (2018): 11407–11414, https://doi.org/10.1021/acsomega.8b01524.

57. D. Shivakumar, J. Williams, Y. Wu, W. Damm, J. Shelley, and W. Sherman, "Prediction of Absolute Solvation Free Energies Using Molecular Dynamics Free Energy Perturbation and the OPLS Force Field," *Journal of Chemical Theory and Computation* 6, no. 5 (2010): 1509–1519, https://doi.org/10.1021/ct900587b.

58. E. F. Pettersen, T. D. Goddard, C. C. Huang, et al., "UCSF Chimera—A Visualization System for Exploratory Research and Analysis," *Journal of Computational Chemistry* 25, no. 13 (2004): 1605–1612, https://doi.org/10.1002/jcc.20084.

59. Z. Yang, K. Lasker, D. Schneidman-Duhovny, et al., "UCSF Chimera, MODELLER, and IMP: An Integrated Modeling System," *Journal of Structural Biology* 179, no. 3 (2012): 269–278, https://doi.org/10.1016/j.jsb.2011.09.006.

60. G. Ramage, S. P. Saville, B. L. Wickes, and J. L. López-Ribot, "Inhibition of Candida albicans Biofilm Formation by Farnesol, a Quorum-Sensing Molecule," *Applied and Environmental Microbiology* 68, no. 11 (2002): 5459–5463, https://doi.org/10.1128/AEM.68.11.5459-5463.2002.

61. R. Kovács, and L. Majoros, "Fungal Quorum-Sensing Molecules: A Review of Their Antifungal Effect Against Candida Biofilms," *Journal of Fungi* 6, no. 3 (2020): 99, https://doi.org/10.3390/jof6030099.

62. R. Pirie, H. A. Stanway-Gordon, H. L. Stewart, et al., "An Analysis of the Physicochemical Properties of Oral Drugs From 2000 to 2022," *RSC Medicinal Chemistry* 15, no. 9 (2024): 3125–3132, https://doi.org/10.1039/D4MD00160E.

63. D. Dahlgren, and H. Lennernäs, "Intestinal Permeability and Drug Absorption: Predictive Experimental, Computational and In Vivo Approaches," *Pharmaceutics* 11, no. 8 (2019): 411, https://doi.org/10.3390/pharmaceutics11080411.

64. S. K. Bagal, and P. J. Bungay, "Minimizing Drug Exposure in the CNS While Maintaining Good Oral Absorption," *ACS Medicinal Chemistry Letters* 3, no. 12 (2012): 948–950, https://doi.org/10.1021/ml300378n.

65. A. Singh, P. Somvanshi, and A. Grover, "Pyrazinamide Drug Resistance in RpsA Mutant (Δ438A) of Mycobacterium tuberculosis: Dynamics of Essential Motions and Free-Energy Landscape Analysis," *Journal of Cellular Biochemistry* 120, no. 5 (2019): 7386–7402, https://doi.org/10.1002/jcb.28013.

66. A. Konakchiev, B. Mikhova, M. Todorova, et al., "Composition of the Essential Oil ofAchillea AsplenifoliaVent. From Bulgaria," *Journal of Essential Oil Bearing Plants* 8, no. 3 (2005): 318–323, https://doi.org/10.1080/0972060X.2005.10643459.

67. H. Nogawa, and T. Kawai, "hERG Trafficking Inhibition in Drug-Induced Lethal Cardiac Arrhythmia," *European Journal of Pharmacology* 741 (2014): 336–339, https://doi.org/10.1016/j.ejphar.2014.06.044.

68. S. A. Hollingsworth, and R. O. Dror, "Molecular Dynamics Simulation for All," *Neuron* 99, no. 6 (2018): 1129–1143, https://doi.org/10.1016/j.neuron.2018.08.011.

69. G. P. Kumwenda, W. Kasambara, A. Phiri, et al., "A Multidrug-Resistant Stenotrophomonas maltophilia Clinical Isolate From Kamuzu Central Hospital, Malawi," *Malawi Medical Journal* 33, no. 2 (2021): 82–84, https://doi.org/10.4314/mmj.v33i2.3.

70. D. D. Li, T. T. Wu, P. Yu, et al., "Molecular Dynamics Analysis of Binding Sites of Epidermal Growth Factor Receptor Kinase Inhibitors," *ACS Omega* 5, no. 26 (2020): 16307–16314, https://doi.org/10.1021/acsomega.0c02183.

71. C. Gago, B. Bakchiche, T. Djekhioua, and M. da Graça Miguel, "Cistus ladanifer L.: Essential Oils, Volatiles, By-Products, and Their Biological Properties," *Molecules* 30, no. 22 (2025): , https://doi.org/10.3390/molecules30224425.

72. G. D. Brown, E. R. Ballou, S. Bates, et al., "The Pathobiology of Human Fungal Infections," *Nature Reviews Microbiology* 22, no. 11 (2024): 687–704, https://doi.org/10.1038/s41579-024-01062-w.

73. M. Shafiei, H. Toreyhi, L. Firoozpour, et al., "Design, Synthesis, and In Vitro and In Vivo Evaluation of Novel Fluconazole-Based Compounds With Promising Antifungal Activities," *ACS Omega* 6, no. 38 (2021): 24981–25001, https://doi.org/10.1021/acsomega.1c04016.

74. G. Simon, C. Bérubé, P.-A. Paquet-Côté, D. Grenier, and N. Voyer, "Preventing Candida albicans Biofilm Formation Using Aromatic-Rich Piperazines," *Bioorganic & Medicinal Chemistry* 28, no. 23 (2020): 115810, https://doi.org/10.1016/j.bmc.2020.115810.

75. E. D. Ashley, "Antifungal Drugs: Special Problems Treating Central Nervous System Infections," *Journal of Fungi* 5, no. 4 (2019): 97, https://doi.org/10.3390/jof5040097.

76. D. E. Pires, T. L. Blundell, and D. B. Ascher, "pkCSM: Predicting Small-Molecule Pharmacokinetic and Toxicity Properties Using Graph-Based Signatures," *Journal of Medicinal Chemistry* 58, no. 9 (2015): 4066–4072, https://doi.org/10.1021/acs.jmedchem.5b00104.

77. Y. Zhao, C. Zeng, and M. A. Massiah, "Molecular Dynamics Simulation Reveals Insights Into the Mechanism of Unfolding by the A130T/V Mutations Within the MID1 Zinc-Binding Bbox1 Domain," *Plos One* 10, no. 4 (2015): e0124377, https://doi.org/10.1371/journal.pone.0124377.

78. X. Song, L. Bao, C. Feng, et al., "Accurate Prediction of Protein Structural Flexibility by Deep Learning Integrating Intricate Atomic Structures and Cryo-EM Density Information," *Nature Communications* 15, no. 1 (2024): 5538, https://doi.org/10.1038/s41467-024-49858-x.

79. B. Sathiyamani, E. A. Daniel, S. Ansar, et al., "Structural Analysis and Molecular Dynamics Simulation Studies of HIV-1 Antisense Protein Predict Its Potential Role in HIV Replication and Pathogenesis," *Frontiers in Microbiology* 14 (2023): 1152206, https://doi.org/10.3389/fmicb.2023.1152206.

80. M. M. Costa da Silva, J. Bezerra de Araújo Neto, A. T. Lucas dos Santos, et al., "Antibiotic-Potentiating Activity of the Schinus terebinthifolius Raddi Essential Oil Against MDR Bacterial Strains," *Plants* 12, no. 8 (2023): 1587, https://doi.org/10.3390/plants12081587.

81. T. Budiyanti, W. Nawfetrias, E. Mansyah, N. Indriyani, R. Reninta, and E. Husada, "The Metabolomic Profile of Garcinia intermedia Leaves With Several Sample Drying Methods," *Environmental Science* 1253, no. 1 (2023): 012018, https://doi.org/10.1088/1755-1315/1253/1/012018.

82. N. F. Sianipar, K. Assidqi, Y. E. Hadisaputri, S. Salam, R. Tarigan, and R. Purnamaningsih, "Determination of Bioactive Compounds of Superior Mutant Rodent Tuber (Typhoniumflagelliforme) in Various Fractions Using GC-MS," *Environmental Science* 794, no. 1 (2021): 012144, https://doi.org/10.1088/1755-1315/794/1/012144.

83. V. C. Shanti, and I. Neerakkal, "GC-MS Analysis and In Silico Activity Prediction of Phytocompounds in the Roots of Chrysopogon zizanioides (L.) Roberty," *Plant Science Today* 8, no. 1 (2021): 218–224, https://doi.org/10.14719/pst.2021.8.1.1008.

84. B. Fatima, H. Degaïchia, L. Abdelbaki, and F. Benrebiha, "Evaluation in vitro du potentiel antifongique de l'huile essentielle et des extraits méthanoliques d'une Asteraceae Artémisia Absinthium L," *Agrobiologia* 8 (2018): 886–895.

85. E. E. Saveleva, A. A. Efremov, N. A. Bulgakova, T. V. Rukosueva, and V. A. Volkova, "Antimicrobial Activity of Yarrow Essential Oil Fractions," *Farmaciya* 72, no. 6 (2023): 26–31, https://doi.org/10.29296/25419218-2023-06-04.

86. A. Capuzzo, A. Occhipinti, and M. E. Maffei, "Antioxidant and Radical Scavenging Activities of Chamazulene," *Natural Product Research* 28, no. 24 (2014): 2321–2323, https://doi.org/10.1080/14786419.2014.931393.

87. A. Mathlouthi, N. Saadaoui, and M. Ben-Attia, "Essential Oils From Artemisia Species Inhibit Biofilm Formation and the Virulence of Escherichia coli EPEC 2348/69," *Biofouling* 37, no. 2 (2021): 174–183, https://doi.org/10.1080/08927014.2021.1886278.

Supporting Information

Additional supporting information can be found online in the Supporting Information section. **Supporting Information.** The supporting information contains the amino acid sequence of the CYC protein and the modeling of this protein using SWISS-MODEL, with justification for the choice of the AlphaFold model.